

Original Article
Virology



Establishment of inflammatory model induced by *Pseudorabies virus* infection in mice

Chun-Zhi Ren ^{1,3}, Wen-Yue Hu ², Jin-Wu Zhang ¹, Ying-Yi Wei ¹,
Mei-Ling Yu ^{1,*}, Ting-Jun Hu ^{1,*}

¹College of Animal Science and Technology, Guangxi University, Nanning 530004, PR China

²School of Life Sciences & Biotechnology, Shanghai Jiao Tong University, Shanghai 200030, PR China

³Guangxi Agricultural Vocational College, Nanning 530007, PR China



Received: Oct 5, 2020

Revised: Dec 18, 2020

Accepted: Jan 7, 2021

*Corresponding authors:

Ting-Jun Hu

College of Animal Science and Technology,
Guangxi University, 100 Daxuedong Road,
Xixiangtang District, Nanning 530004, PR
China.

E-mail: tingjunhu@gxu.edu.cn

Mei-Ling Yu


College of Animal Science and Technology,
Guangxi University, 100 Daxuedong Road,
Xixiangtang District, Nanning 530004, PR
China.

E-mail: yumeling@gxu.edu.cn


© 2021 The Korean Society of Veterinary
Science

This is an Open Access article distributed
under the terms of the Creative Commons
Attribution Non-Commercial License ([https://
creativecommons.org/licenses/by-nc/4.0](https://creativecommons.org/licenses/by-nc/4.0))
which permits unrestricted non-commercial
use, distribution, and reproduction in any
medium, provided the original work is properly
cited.


ORCID iDs

Chun-Zhi Ren 


<https://orcid.org/0000-0003-3894-8641>

Wen-Yue Hu 

<https://orcid.org/0000-0003-0362-1577>

Jin-Wu Zhang 

<https://orcid.org/0000-0002-4675-7039>

Ying-Yi Wei 

<https://orcid.org/0000-0001-6220-6563>

ABSTRACT

Background: *Pseudorabies virus* (PRV) infection leads to high mortality in swine. Despite extensive efforts, effective treatments against PRV infection are limited. Furthermore, the inflammatory response induced by PRV strain GXLB-2013 is unclear.

Objectives: Our study aimed to investigate the inflammatory response induced by PRV strain GXLB-2013, establish an inflammation model to elucidate the pathogenesis of PRV infection further, and develop effective drugs against PRV infection.

Methods: Kunming mice were infected intramuscularly with medium, LPS, and different doses of PRV-GXLB-2013. Viral spread and histopathological damage to brain, spleen, and lung were determined at 7 days post-infection (dpi). Immune organ indices, levels of reactive oxygen species (ROS), nitric oxide (NO), and inflammatory cytokines, as well as levels of activity of COX-2 and iNOS were determined at 4, 7, and 14 dpi.

Results: At 10^5 – 10^6 TCID₅₀ PRV produced obviously neurological symptoms and 100% mortality in mice. Viral antigens were detectable in kidney, heart, lung, liver, spleen, and brain. In addition, inflammatory injuries were apparent in brain, spleen, and lung of PRV-infected mice. Moreover, PRV induced increases in immune organ indices, ROS and NO levels, activity of COX-2 and iNOS, and the content of key pro-inflammatory cytokines, including interleukin (IL)-1 β , IL-6, tumor necrosis factor- α , interferon- γ and MCP-1. Among the tested doses, 10^2 TCID₅₀ of PRV produced a significant inflammatory mediator increase.

Conclusions: An inflammatory model induced by PRV infection was established in mice, and 10^2 TCID₅₀ PRV was considered as the best concentration for the establishment of the model.

Keywords: *Pseudorabies virus*; inflammatory; cytokines; mice

INTRODUCTION

Pseudorabies virus (PRV), which belongs to the family *Herpesviridae*, subfamily *Alphaherpesvirinae*, is the main pathogen that causes Aujeszky's disease (AD) [1]. In addition to pigs, PRV can infect most mammals, such as cattle, sheep, rodents, dogs, and a wide range of wildlife. PRV is related to human pathogens such as herpes simplex virus 1 (HSV-1) and varicella-zoster virus (VZV) [2], and since 2018, PRV infection in humans has been identified at the genetic

Mei-Ling Yu 
<https://orcid.org/0000-0002-9517-9802>
Ting-Jun Hu 
<https://orcid.org/0000-0002-6010-8342>

Funding

This work was financially supported by the National Natural Science Fund of China (Grant number: 32072907); Innovation Project of Guangxi Graduate Education (Grant number: YCBZ2020004).

Conflict of Interest

The authors declare no conflicts of interest.

Author Contributions

Conceptualization: Ren CZ, Hu WY, Yu ML;
Data curation: Hu WY, Zhang JW; Formal
analysis: Ren CZ, Yu ML; Investigation: Hu
TJ, Ren CZ, Hu WY, Zhang JW, Yu ML; Project
administration: Hu TJ; Writing - original draft:
Ren CZ, Yu ML; Writing - review & editing: Hu
TJ, Wei YY.

level [3,4]. These observations demonstrate that PRV has pathogenicity to humans [4,5], indicating it is worth additional research attention.

PRV always causes reproductive failure in pregnant sows; encephalitis, lung inflammation and high mortality in newborn piglets; and severe, uncontrollable pruritus and lethal neuropathy in non-natural hosts [6-8]. Vaccination is an available strategy for the prevention of PRV infection [9]; however, the commercially available vaccine against PRV is a potential health risk for other animals [10]. Despite the eradication of *Pseudorabies* from domestic pigs in some developed countries [11], in China, herds immunized with the Bartha-K61 vaccine were shown to be infected with highly virulent PRV variants since late 2011, resulting in severe socioeconomic consequences [12-14]. Moreover, variant PRV is currently the most prevalent genotype worldwide, and most commonly involved in cross-species transmission events [5,15,16]. Therefore, development of a safe and highly efficient vaccine or drugs against PRV is of great importance.

A suitable animal model of PRV infection would be useful in further elucidating the pathogenesis of PRV infection and developing effective ant-PRV vaccines and drugs [17]. As observed in neonatal piglets, when PRV infects mice, the virus enters peripheral neurons and propagates to the central nervous system, resulting in brain lesions [18,19]. A mouse model could be a key platform for the study of PRV infection. There have been reports describing the infection route, clinical signs, viral distribution, lesion patterns, and vaccination of PRV in pigs and mice, but there is limited information on the inflammatory response in PRV-infected mice. Moreover, encephalitis caused by PRV infection is a key factor contributing to animal death [20]. To establish an inflammatory response model, Kunming mice were selected for infection with PRV-GXLB-2013. The immune organ indices, inflammatory injuries of organs, and the levels of inflammatory mediators, as well as the content level of key pro-inflammatory cytokines, were investigated to elucidate the PRV-induced inflammatory response in Kunming mice.

MATERIALS AND METHODS

Chemicals and reagents

LPS was purchased from Sigma Chemical Co. Ltd. (USA). Dulbecco's modified Eagle medium (DMEM) and fetal bovine serum (FBS) were purchased from Gibco (USA). Commercial kits for biochemical analysis of interleukin-1 β (IL-1 β), IL-6, tumor necrosis factor- α (TNF- α), interferon- γ (IFN- γ), reactive oxygen species (ROS), nitric oxide (NO), inducible nitric oxide synthase (iNOS), and Cyclooxygenase-2 (Cox-2) were obtained from Nanjing Jiancheng Bioengineering Institute (China). Anti-PRV monoclonal antibody (PRV-mcab) was purchased from Chundu Biotechnology (China).

Virus and cells

Pseudorabies virus (PRV) strain GXLB-2013 was kindly provided by the laboratory of Preventive Veterinary Medicine, Guangxi University. Porcine kidney 15 (PK15) cells were purchased from the American Type Culture Collection (USA). The cells were cultured in DMEM supplemented with 10% FBS at 37°C under 5% CO₂. The GXLB-2013 PRV strain was propagated in PK15 cells, and the 50% tissue culture infective dose (TCID₅₀) values for PRV were determined by following the Reed-Muench method. The titer of PRV-GXLB-2013 was determined to be 10^{7.2} TCID₅₀ for the following experiments.

Animals and treatment

The experimental protocol was approved by the Institution Animal Ethics Committee of Guangxi University. Housing and experimental treatment of animals were performed in accordance with National Institute of Health Guidelines (Institute of Laboratory Animal Resources, 1996). Two hundred and ten specific-pathogen-free (SPF) Kunming mice (4 weeks, 18–22 g) of either sex were purchased from the Laboratory Animal Center of Guangxi Medical University, China (SYXK Gui 2014-0003), and maintained under SPF conditions for one week with free access to a standard chow diet and water. The 210 SPF Kunming mice were randomly divided into 7 groups (3 replicates of 10 mice): Control, LPS, and 10^2 – 10^6 TCID₅₀ PRV groups. Ten samples from all groups were collected for analysis on days 4, 7, and 14 post-infection.

Mice were infected intramuscularly with 100 μ L of cell culture supernatant from PK15 cells, LPS (1 mg/kg body weight), or different PRV titers (10^2 – 10^6 TCID₅₀ PRV). After infection, clinical symptoms of mice were observed daily. Mice were sacrificed by injection of 200 mg/kg of pentobarbital, and brains, lungs, thymus, spleens, hearts, livers, and kidneys were obtained from the sacrificed mice. Half of all tissue specimens were fixed in 4% paraformaldehyde for histopathologic analysis, and the other half were stored at -20°C until use.

Determination of viral spread by PCR

The brain, lung, thymus, spleen, heart, liver, and kidney of mice were collected at 7 days post-infection (dpi) and examined to establish the presence of PRV virus by PCR. Briefly, total DNA was isolated from organ tissue by Genomic DNA Extraction Kit (TaKaRa, Japan). The forward and reverse primers 5'-CGGCTTCCACTCGCAGCTCTTCTC-3' and 5'-TGTGGGTCATCACGAGCACGTACAGC-3' respectively, were used to amplify a 388-bp fragment of the glycoprotein E gene of PRV (GenBank accession no. MK622291.1).

Histopathology and immunohistochemistry

At 7 dpi, brain, spleen, and lung tissues were collected and fixed; subsequently, tissues were enclosed in paraffin wax and cut to form 3 μ m thick slices. For light microscopical investigation, sections underwent hematoxylin and eosin (H&E) staining before analysis under an optical microscope (Nikon eclipse 80i, Japan). Three slides from different parts of each tissue type (3 mice per group) were analyzed. For immunohistochemical analysis, sections of brain were dewaxed and rehydrated. Intrinsic peroxidase activity was blocked via 3% hydrogen peroxide (Merck, Germany) treatment for 10 min. Sections were then incubated with undiluted normal goat serum for 30 min to block nonspecific binding sites before incubation with the primary antibody. After washing with Tris-buffered saline (TBS), the primary monoclonal antibody against PRV (ChunDu, China; 1:500 diluted in TBS, 60 min) was used to detect PRV-infected cells. Sections were rinsed and subsequently incubated with a biotinylated goat anti-rabbit IgG (Vector Laboratories, USA; diluted 1:200 in TBS, 30 min), followed by incubation with ABC (Vector) diluted 1:10 in TBS for 30 min. The DAB chromogenic agent were added into the sections until the cells were stained, then 0.01M sterile phosphate-buffered saline (PBS) was added to terminate the reaction.

Measurement of immune organs indices

Mice were weighed before being sacrificed at 4, 7, and 14 dpi, after which immune organs, including spleen and thymus, were immediately removed and weighed. The organ index was calculated as the organ weight (mg) divided by body weight (g).

Measurement of ROS and NO level in spleen

Splenocytes from mice of each group were prepared for ROS analysis by incorporating the fluorescent probe of DCFH-DA as previously described [21]. Briefly, 100 μL of splenocytes (1×10^6 cells/mL) were transferred to a black 96-well plate. After adherence, the cells were incubated with the DCFH-DA ROS fluorescent probe (10 μM) at 37°C for 30 min. Then, the cells were washed three times with sterile phosphate-buffered saline (PBS), and fluorescent intensity was measured at 488 nm (excitation) and 525 nm (emission) on an automatic microplate reader (TECAN, Switzerland). The secretion of NO was detected according to the manufacturer's instructions. Briefly, spleen tissues were homogenized in normal saline (1:9, V/V) with an Ultra-Turrax T25 Homogenizer. After centrifugation at $10,000 \times g$ for 15 min at 4°C, the supernatant was examined to determine the NO concentration level; absorbance at 550 nm was measured on an automatic microplate reader.

Measurement of COX-2 and iNOS activity in spleen

Spleen tissues were homogenized in normal saline (1:9, V/V). After centrifugation of the homogenate at $10,000 \times g$ for 15 min at 4°C, the supernatant was used, according to the manufacturer's instructions, to determine the activities of COX-2 and iNOS.

Cytokine analysis

Spleen tissues were homogenized in normal saline (1:9, V/V). After centrifugation of the homogenate at $10,000 \times g$ for 15 min at 4°C, the supernatants were collected for quantitative detection of cytokines (IL-1 β , IL-6, TNF- α , IFN- γ , and MCP-1) using commercial ELISA kits and following the manufacturers' instructions. Optical density at 450 nm (OD₄₅₀) was measured using a Multimode Plate Reader (PerkinElmer Instruments, Switzerland).

Statistical analysis

Statistical analyses were performed using SPSS version 21.0. All data were expressed as mean \pm SD. One-way analysis of variance was used for the determination of differences in measurements between groups. A result with a *p* value < 0.05 indicated a significant difference, while *p* < 0.01 indicated a highly significant difference.

RESULTS

Clinical symptoms and mortality of PRV-GXLB-2013 infection

Mice infection with 10^5 – 10^6 TCID₅₀ PRV-GXLB-2013 exhibited several clinical symptoms, including agitation, pruritus, scratching and gnawing the facial skin, skin lesions with tissue damage, and bleeding. Neurological symptoms could also be observed and symptoms became apparent about 12 h before death. All mice in the 10^5 – 10^6 TCID₅₀ PRV group died at 3 or 4 dpi, while 20% of the mice in 10^4 TCID₅₀ PRV group died at 4 dpi. A survival curve is shown in Fig. 1. Clinical symptoms were not evident in mice of the 10^2 and 10^3 TCID₅₀ PRV groups, and 100% of the mice in those groups survived. The control group mice appeared to be in a good mental state, exhibiting active behavior, bright hair color, and normal appetite.

Detection of viral antigen in mice at 7 day post infected with PRV-GXLB-2013

To detect viral spread, tissue sections underwent PCR and immunohistochemical analyses using an anti-PRV monoclonal antibody. In mice infected with different doses of PRV-GXLB-2013, viral antigens were detectable in kidney, heart, lung, liver, spleen, and brain. PCR-based identification of viral antigens in mice infected with 10^2 TCID₅₀ PRV is shown in

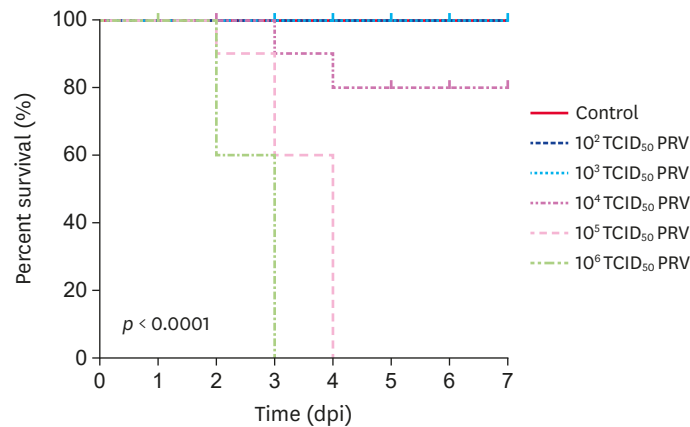


Fig. 1. The mortality of PRV-infected mice. Survival curves ($n = 30$ in each group) in Kunming mice after intramuscular infection with different doses of PRV (10^2 – 10^6 TCID₅₀ PRV per mouse). The X-axis presents the days post-injection, and the Y-axis indicates the survival rate of the PRV-infected mice. The survival rate was monitored for up to 7 dpi and was calculated using SPSS. $p < 0.01$ indicates a significant difference. PRV, *Pseudorabies virus*.

Fig. 2A. Fragments of gene gE (approximately 388 bp) were amplified from kidney, heart, lung, liver, spleen, and brain tissues. The brain tissue of mice infected with PRV showed massive antigen staining (**Fig. 2B**).

The effects of PRV infection on organ damage

Results of H&E staining of brain, lung, and spleen tissues are shown in **Fig. 3**. Normal histological structures were observed in the brain, lung, and spleen of mice in the control group. However, PRV infection induced histopathological changes in brain tissue that included tubular infiltration, neuronal degeneration, hemorrhage, satellitosis, neuronophagy, and reactive gliosis, whereas the LPS treatment induced marked tubular infiltration and neuronophagy. In the lungs of the PRV-infected group, the lung alveolar structure was missing, and inflammatory cell infiltration, hemorrhage, and congestion were observed. For mice in the LPS group, there was slight hemorrhaging observed in the lungs. In

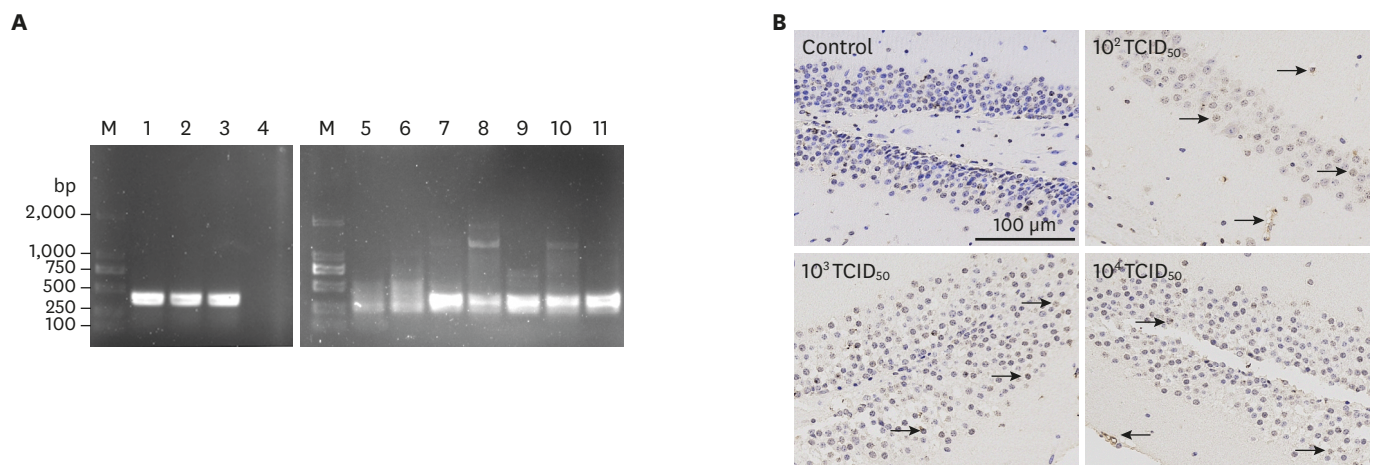


Fig. 2. Detection of viral antigens in mice infected with PRV-GXLB-2013. Panel A: PCR-based identification of PRV in mice infected with 10^2 TCID₅₀ PRV. Lane M, DNA Mark 2000; lanes 1–3, 11: PRV propagated in PK-15 cells; lane 4, negative control; 5, kidney; lane 6, heart; lane 7, lung; lane 8, liver; lane 9, spleen; lane 10, brain. Panel B: identification of PRV in brain tissue based on immunohistochemistry analysis (anti-PRV monoclonal antibody). Arrows indicate positively stained cells. PRV, *Pseudorabies virus*.

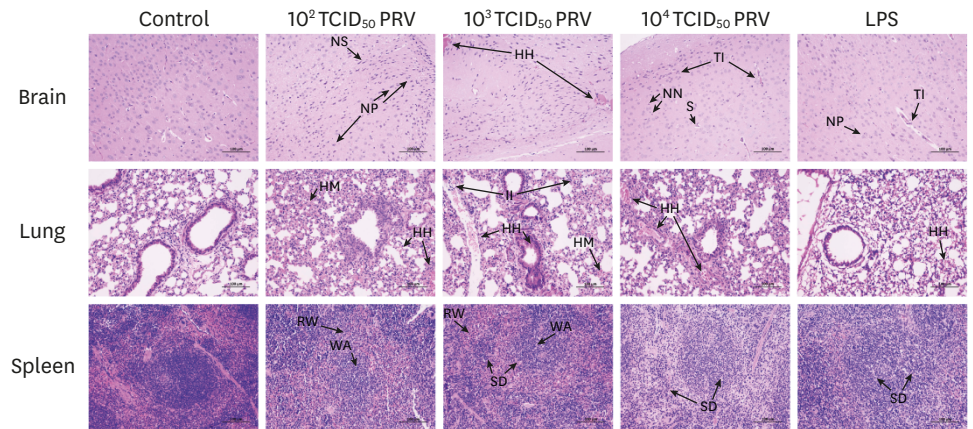


Fig. 3. Histopathological changes in tissues of mice infected with PRV-GXLB-2013. Paraffin sections of brain, lung, and spleen tissues from control, 10^2 – 10^4 TCID₅₀ PRV, and LPS groups were stained with hematoxylin and eosin. Final magnification $\times 200$, bars = 100 μ m. Representative images are shown. PRV, *Pseudorabies virus*; N, neurons; G, glial cells; NN, necrotic neurons; NP, neuronophagia; TI, tubular infiltration; S, satellitosis; HH, hemorrhage; HM, hyperemia; NS, shrinkage of neurons; II, infiltration of inflammatory cell; RW, red pulp widened; WA, white pulp atrophied; SD, splenic corpuscles destroyed.

the spleens of the PRV-infected and LPS-treated mice, reduction and disappearance of splenic corpuscles were observed, red pulp was widened, and white pulp was atrophied.

The effects of PRV infection on organ indices

Spleen and thymus are important immune organs, and their weights are indicative of a relative or absolute overall rating of immune function [14]. Compared with the control group, mice of the 10^2 – 10^4 TCID₅₀ PRV groups had increased thymus and spleen indices (**Fig. 4**). At 4 dpi, the thymus index in the 10^3 TCID₅₀ group was significantly higher than that in the control group ($p < 0.05$). Moreover, at 14 dpi, the thymus index in the 10^4 TCID₅₀ group was significantly higher than that in the control group ($p < 0.05$). The spleen index in the 10^4 TCID₅₀ group was significantly higher than that in the control group at 4 dpi and 7 dpi.

The effects of PRV infection on ROS and NO levels

ROS and NO are important inflammatory mediators. The level of ROS in the 10^2 TCID₅₀ PRV group was significantly higher than that in the control group at 4, 7, and 14 dpi ($p < 0.05$). At 7 dpi, the levels of ROS in the PRV-infected and LPS-treated groups were significantly higher

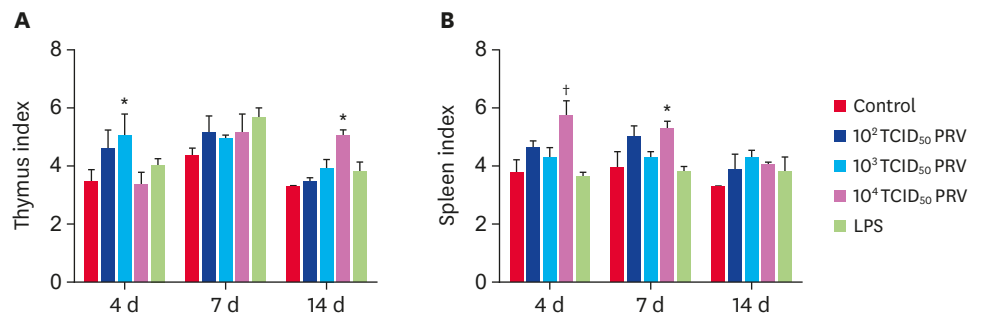


Fig. 4. Effect of PRV-GXLB-2013 on thymus (A) and spleen (B) indices. The organ indices were measured at 4, 7, and 14 dpi, and were calculated as organ weight (mg) divided by bodyweight (g). Data are mean \pm SD. PRV, *Pseudorabies virus*. * $p < 0.05$, † $p < 0.01$ vs. control group (n = 6).

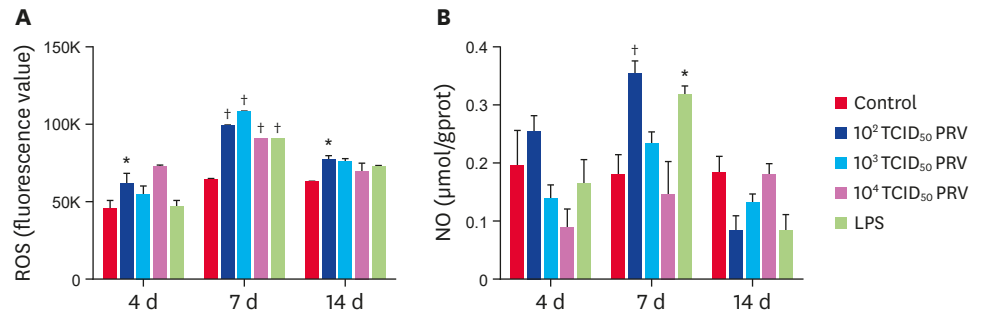


Fig. 5. Effect of PRV-GXLB-2013 on ROS and NO levels in mouse spleen. The levels of ROS (A) and NO (B) were measured at 4, 7, and 14 dpi. Data are mean \pm SD.

PRV, *Pseudorabies virus*.

* $p < 0.05$, † $p < 0.01$ vs. control group (n = 6).

than that in the control group ($p < 0.01$) (Fig. 5A). The levels of NO in the 10^2 TCID₅₀ PRV group and the LPS group were significantly higher than that in the control group at 7 dpi ($p < 0.05$) (Fig. 5B).

The effects of PRV infection on COX-2 and iNOS activity

The PRV-GXLB-2013 infection produced increases in COX-2 and iNOS activity levels (Fig. 6). At 7 dpi, the activity of COX-2 and iNOS in the 10^2 TCID₅₀ and 10^3 TCID₅₀ PRV groups were significantly higher than those in the control group ($p < 0.05$). The activity of COX-2 in the 10^2 TCID₅₀ PRV group was significantly higher than that in the control group at 14 dpi ($p < 0.05$).

The effects of PRV infection on cytokine secretions

The PRV-GXLB-2013 infection strongly increased the levels of IL-1 β , IL-6, TNF- α , IFN- γ , and MCP-1 (Fig. 7). Compared with the control group, the levels of MCP-1 in all treated groups were significantly higher at 7 dpi ($p < 0.05$); moreover, the levels of IL-1 β , IL-6, TNF- α and MCP-1 in the 10^2 TCID₅₀ PRV group were significantly increased at 7 dpi ($p < 0.05$), while the levels of IL-6 and TNF- α in the 10^2 TCID₅₀ PRV group were significantly increased at 14 dpi ($p < 0.05$). The 10^4 TCID₅₀ PRV treatment induced high levels of IL-1 β , IFN- γ , and MCP-1 at 14 dpi; in addition, the LPS treatment induced high levels of TNF- α and MCP-1.

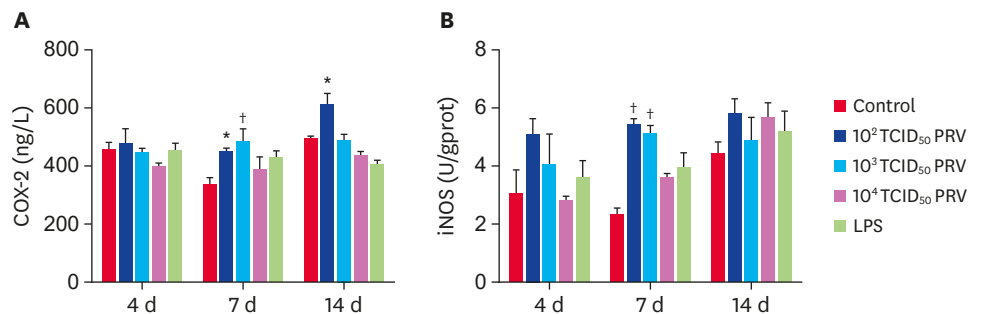


Fig. 6. Effect of PRV-GXLB-2013 on the activity of COX-2 and iNOS in mouse spleen. The levels of COX-2 (A) and iNOS (B) were measured at 4, 7, and 14 dpi. Data are mean \pm SD.

PRV, *Pseudorabies virus*.

* $p < 0.05$, † $p < 0.01$ vs. control group (n = 6).

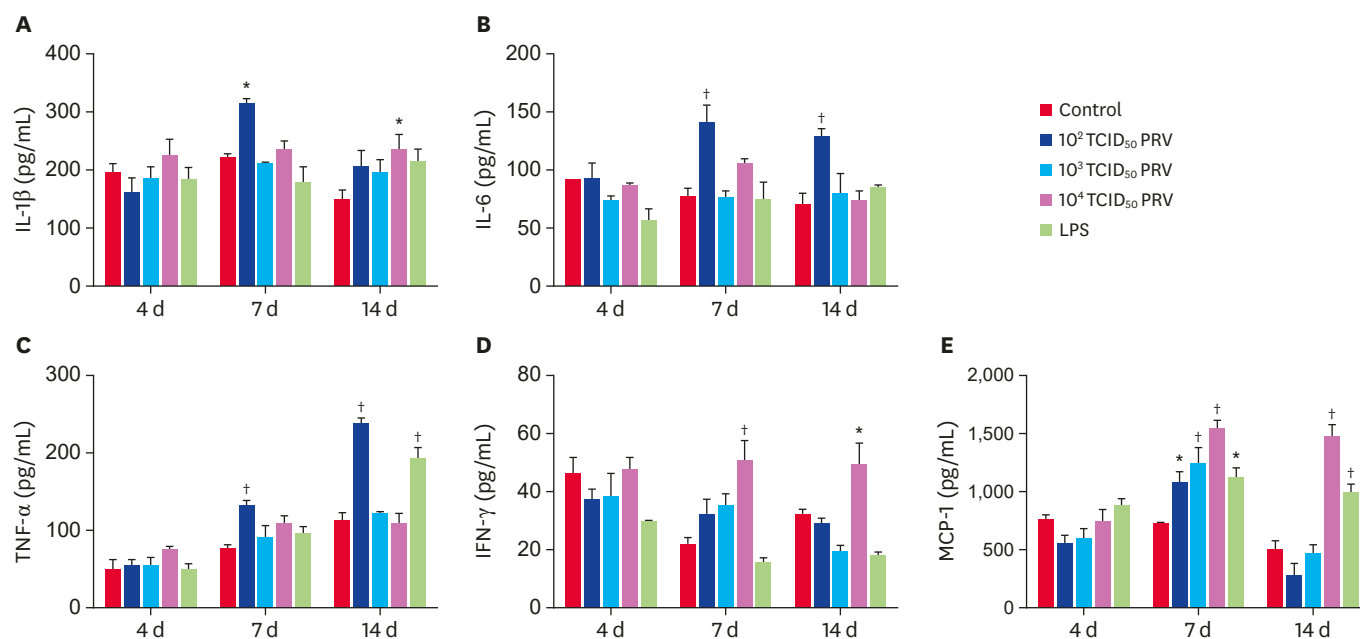


Fig. 7. Concentrations of IL-1 β (A), IL-6 (B), TNF- α (C), IFN- γ (D), and MCP-1 (E) in mouse spleen. Five cytokines in the spleens of injected mice were assayed at 4, 7, and 14 dpi. Data are mean \pm SD.

IL, interleukin; TNF, tumor necrosis factor; IFN, interferon.

* $p < 0.05$, † $p < 0.01$ vs. control group ($n = 6$).

DISCUSSION

PRV causes reproductive failure, diarrhea, encephalitis, severe pruritus, and high mortality in a wide range of hosts and causes considerable economic losses in animal husbandry [6,7,8,10]. The PRV variants isolated from farms in China show insertion, deletion, or substitution of amino acids at key sites in several virulence genes [12,13]. PRV-GXLB-2013, which was isolated from Guangxi province in 2013 and used in this study, was shown to have pathogenicity to BALB/c mice stronger than that of the Bartha-K61 strain [22]. However, prior to this study, the inflammatory response induced by PRV-GXLB-2013 was unclear. This study demonstrated that PRV-GXLB-2013 in Kunming mice results in death, encephalitis, inflammatory injuries of lung, brain, and spleen, increased immune organ indices, and increases in the levels of inflammatory factors, pro-inflammatory cytokines, and chemokines. Thus, this mouse inflammation model could be used to screen drugs potentially effective against PRV infection.

Encephalitis caused by PRV infection can result in severe neurological defects and death in swine [6,20]. It has been reported that PRV induces encephalitis in both pigs and mice and produces similar pathological signs [20]. Herein, we demonstrated that 10⁴–10⁶ TCID₅₀ of PRV-GXLB-2013 is lethal for Kunming mice, with mouse mortality rates increasing with the increase in the applied dose of virus. Mice infected with PRV-GXLB-2013 showed localized pruritus and lesions, observations in accordance with previous reports showing that mice are unable to survive an acute PRV infection [7,23,24]. In addition, histopathological examination revealed that PRV-GXLB-2013 infection leads to encephalitis, as evidenced by the perivascular cuff-like changes, neuronal degeneration, shrinkage and necrosis, infiltration of inflammatory cells, and extensive glial cell necrosis in the brain. These histopathological changes provided morphological data supporting the clinical neurological signs in mice

after PRV infection. Our results are consistent with those in previous studies, which showed that PRV could induce the activation of microglia and macrophages and the infiltration of leukocytes in mice [17]. Virus distribution is an important and directly measurable parameter to evaluate virus infection *in vivo* [17]. Brittle et al. [19] reported that PRV can be detected in brain, lung, kidney, spleen, pancreas, stomach, liver, heart, and urinary bladder at 70 h and 192 h after PRV infection. Our results showed that a specific gene gE fragment was detectable in brain, spleen, lung, liver, and kidney at 7 dpi, and was evident in lung, spleen, and brain. These results were consistent with those in a previous report indicating the nervous and respiratory systems are the main target organs of PRV [17]. The virus distribution results revealed that PRV-GXLB-2013 could infect Kunming mice and propagate in major organs. The distribution of virus in brain tissue was positively linked to the clinical parameters and histopathological changes observed in infected mice.

The host's inflammatory response is important in preventing the spread of viral infections [25]. An uncontrolled inflammatory response often leads to a damaging systemic inflammation, also known as a "cytokine storm," that can be fatal for the host [24,26]. A viral infection can result in an excessive inflammatory response and can induce the generation of pro-inflammatory factors such as free radicals and cytokines, which have crucial roles in the pathogenesis of some diseases [27,28]. Although it was reported that a PRV-Bartha infection did not induce a specific and lethal systemic inflammatory response [24], a PRV-GXLB-2013 infection does induce an excessive inflammatory response leading to death in mice, as evidenced by the increased secretions of NO, ROS, iNOS, COX-2, IL-1 β , IL-6, TNF- α and MCP-1 and the increased organ indices. Additionally, mice infected with PRV-GXLB-2013 showed massive inflammatory cell infiltration in brain, spleen, and lung.

Interestingly, the inflammation caused by PRV was not apparent at 4 dpi, but was evident at 7 and 14 dpi. Moreover, among the tested doses, 10^2 TCID₅₀ was shown to induce a suitable inflammatory response level. The levels of cytokines and chemokines in 10^3 TCID₅₀ and 10^4 TCID₅₀ PRV group were increased but not notably, which may be related to the level of tissue damage and cell destruction caused by the higher viral concentration. In the early period of PRV infection (4 dpi), the level of ROS was increased, and at 7 dpi, the level of ROS was significantly increased in all PRV groups. ROS have an important role in the initiation and development of inflammation and produce oxidative damage to cells, aggravating the virus infection and making the body produce excessive amounts of inflammatory mediators [1,29-32]. At 7 dpi, the NO, iNOS, and COX-2 levels were significantly increased in the 10^2 TCID₅₀ PRV group. Large amounts of NO, generated primarily by iNOS, can be toxic and pro-inflammatory [32,33]. Induction of iNOS can be initiated by the inflammatory cytokines IFN- γ , TNF- α , or IL-1, producing excessive NO, triggering an inflammatory cascade, and leading to tissue and endothelial damage [34,35].

IL-1 β , IL-6, TNF- α and MCP-1 are important pro-inflammatory cytokines [36-39], and the levels of these pro-inflammatory cytokines were increased in mice in the 10^2 TCID₅₀ PRV group at 7 dpi. MCP-1, mainly induced by endogenous inflammatory factors such as IL-1 and TNF- α , can directly lead to the production of large levels of IL-1, IL-6, TNF- α , and other cytokines, and these cytokines, in turn, can stimulate cells to secrete more MCP-1, ultimately leading to a vicious cycle [40]. Notably, our results showed that the level of MCP-1 was significantly increased in all PRV groups. While the level of IFN- γ was not increased in the 10^2 TCID₅₀ PRV group, it was increased in the 10^4 TCID₅₀ PRV group at 7 dpi and 14 dpi. As the PRV infection dose increased, the body's immunity was enhanced, and the level of

IFN- γ in the 10^4 TCID₅₀ group was significantly higher than that in the control group at 7 dpi and 14 dpi. Herein, we demonstrated that a 10^2 TCID₅₀ dose of PRV induces a higher level of inflammatory mediators at 7 dpi than that in the control group, and it produced a better effect than the other PRV concentrations and that of LPS.

Surprisingly, LPS, which is reported to be responsible for the development of the Systemic Inflammatory Response Syndrome in the course of sepsis due to Gram-negative bacterial infection [32], only induced increased levels of ROS, NO, and MCP-1 at 7 dpi, but there were increased levels of TNF- α and MCP-1 at 14 dpi. This result may be related to the injection procedure and sampling time. It has been reported that LPS usually causes an acute inflammatory response [41]. Moreover, LPS-injected mice were reported to show signs of moderate to severe distress, which peaked between days 1 to 3 after injection and gradually resolved within 3 to 5 days after injection [42]. In our previous study, some mice injected with 2.5 mg/kg body weight of LPS twice died at 3 dpi and, all mice were dead at 6 dpi. Considering that the latent period of PRV infection is about 3 days, our study aimed to investigate the inflammatory response induced by PRV to develop effective anti-PRV drugs. To persistently observe inflammation caused by LPS, mice were injected once with LPS (1 mg/kg body weight). Based on the levels of inflammatory mediators, an LPS dose of 1 mg/kg body weight could cause inflammation; however, the inflammatory reaction was lower at 4, 7, and 14 dpi. Thus, the mice in our LPS group did not exhibit inflammatory responses under most conditions. In addition, the inflammation mechanisms associated with viral and bacterial infections differ. Although LPS had a limited role in this study, the level of the inflammatory response induced by LPS could be useful as a reference level.

In conclusion, high doses of PRV-GXLB-2013 (10^5 – 10^6 TCID₅₀ PRV) caused obvious neurological symptoms and 100% mortality in mice, with viral antigens shown to have spread into kidney, heart, lung, liver, spleen, and brain tissues. In addition, inflammatory injuries were evident in the brain, spleen, and lung tissues of mice infected with PRV. A PRV-GXLB-2013 infection can induce inflammatory responses in Kunming mice, and PRV-GXLB-2013 at a titer of 10^2 TCID₅₀ produces a significant increase in inflammatory mediators, including ROS, NO, COX-2, iNOS, IL-1 β , IL-6, TNF- α , and MCP-1. In this study, a PRV infection-induced mouse-inflammatory model was established and based on the clinical manifestations, mortality rate, viral spreading, and inflammatory responses the mouse model meets the requirements of a PRV disease model. Among the tested doses, a 10^2 TCID₅₀ PRV injection was considered the most appropriate for establishing the disease model. The establishment of this model lays a foundation for further research investigating the pathogenesis of PRV and screening for drugs that are effective against PRV infection.

ACKNOWLEDGMENTS

We thank Dr. Huang Weijian in the Laboratory of Animal Infectious Disease in College of Animal Science and Technology at Guangxi University for his kindness in providing the PRV.

REFERENCES

1. Müller T, Hahn EC, Tottewitz F, Kramer M, Klupp BG, Mettenleiter TC, et al. Pseudorabies virus in wild swine: a global perspective. *Arch Virol*. 2011;156(10):1691-1705.
[PUBMED](#) | [CROSSREF](#)

2. Laval K, Enquist LW. The neuropathic itch caused by pseudorabies virus. *Pathogens*. 2020;9(4):E254.
[PUBMED](#) | [CROSSREF](#)
3. Ai JW, Weng SS, Cheng Q, Cui P, Li YJ, Wu HL, et al. Human endophthalmitis caused by pseudorabies virus infection, China, 2017. *Emerg Infect Dis*. 2018;24(6):1087-1090.
[PUBMED](#) | [CROSSREF](#)
4. Hu F, Wang J, Peng XY. Bilateral necrotizing retinitis following encephalitis caused by the pseudorabies virus confirmed by next-generation sequencing. *Ocul Immunol Inflamm*. 2020:1-4.
[PUBMED](#) | [CROSSREF](#)
5. He W, Auclert LZ, Zhai X, Wong G, Zhang C, Zhu H, et al. Interspecies transmission, genetic diversity, and evolutionary dynamics of pseudorabies virus. *J Infect Dis*. 2019;219(11):1705-1715.
[PUBMED](#) | [CROSSREF](#)
6. Wang Y, Xia SL, Lei JL, Cong X, Xiang GT, Luo Y, et al. Dose-dependent pathogenicity of a pseudorabies virus variant in pigs inoculated via intranasal route. *Vet Immunol Immunopathol*. 2015;168(3-4):147-152.
[PUBMED](#) | [CROSSREF](#)
7. Takahashi H, Yoshikawa Y, Kai C, Yamanouchi K. Mechanism of pruritus and peracute death in mice induced by pseudorabies virus (PRV) infection. *J Vet Med Sci*. 1993;55(6):913-920.
[PUBMED](#) | [CROSSREF](#)
8. Sehl J, Teifke JP. Comparative pathology of pseudorabies in different naturally and experimentally infected species—a review. *Pathogens*. 2020;9(8):E633.
[PUBMED](#) | [CROSSREF](#)
9. Colomer MA, Margalida A, Fraile L. Vaccination is a suitable tool in the control of Aujeszky's disease outbreaks in pigs using a population dynamics P systems model. *Animals (Basel)*. 2020;10(5):E909.
[PUBMED](#) | [CROSSREF](#)
10. Lin W, Shao Y, Tan C, Shen Y, Zhang X, Xiao J, et al. Commercial vaccine against pseudorabies virus: a hidden health risk for dogs. *Vet Microbiol*. 2019;233:102-112.
[PUBMED](#) | [CROSSREF](#)
11. Hahn EC, Fadl-Alla B, Lichtensteiger CA. Variation of Aujeszky's disease viruses in wild swine in USA. *Vet Microbiol*. 2010;143(1):45-51.
[PUBMED](#) | [CROSSREF](#)
12. Yu ZQ, Tong W, Zheng H, Li LW, Li GX, Gao F, et al. Variations in glycoprotein B contribute to immunogenic difference between PRV variant JS-2012 and Bartha-K61. *Vet Microbiol*. 2017;208:97-105.
[PUBMED](#) | [CROSSREF](#)
13. Wang T, Tong W, Ye C, Yu Z, Chen J, Gao F, et al. Construction of an infectious bacterial artificial chromosome clone of a pseudorabies virus variant: reconstituted virus exhibited wild-type properties *in vitro* and *in vivo*. *J Virol Methods*. 2018;259:106-115.
[PUBMED](#) | [CROSSREF](#)
14. Liu J, Chen C, Li X. Novel Chinese pseudorabies virus variants undergo extensive recombination and rapid interspecies transmission. *Transbound Emerg Dis*. 2020;67(6):2274-2276.
[PUBMED](#) | [CROSSREF](#)
15. Ye C, Guo JC, Gao JC, Wang TY, Zhao K, Chang XB, et al. Genomic analyses reveal that partial sequence of an earlier pseudorabies virus in China is originated from a Bartha-vaccine-like strain. *Virology*. 2016;491:56-63.
[PUBMED](#) | [CROSSREF](#)
16. Liu Q, Wang X, Xie C, Ding S, Yang H, Guo S, et al. A novel human acute encephalitis caused by pseudorabies virus variant strain. *Clin Infect Dis*. 2020;ciaa987.
[PUBMED](#) | [CROSSREF](#)
17. Zhao X, Tong W, Song X, Jia R, Li L, Zou Y, et al. Antiviral effect of resveratrol in piglets infected with virulent pseudorabies virus. *Viruses*. 2018;10(9):E457.
[PUBMED](#) | [CROSSREF](#)
18. Kim JS, Enquist LW, Card JP. Circuit-specific coinfection of neurons in the rat central nervous system with two pseudorabies virus recombinants. *J Virol*. 1999;73(11):9521-9531.
[PUBMED](#) | [CROSSREF](#)
19. Brittle EE, Reynolds AE, Enquist LW. Two modes of pseudorabies virus neuroinvasion and lethality in mice. *J Virol*. 2004;78(23):12951-12963.
[PUBMED](#) | [CROSSREF](#)
20. Li X, Zhang W, Liu Y, Xie J, Hu C, Wang X. Role of p53 in pseudorabies virus replication, pathogenicity, and host immune responses. *Vet Res (Faisalabad)*. 2019;50(1):9.
[PUBMED](#) | [CROSSREF](#)

21. Chen HL, Yang J, Fu YF, Meng XN, Zhao WD, Hu TJ. Effect of total flavonoids of *Spatholobus suberectus* Dunn on PCV2 induced oxidative stress in RAW264.7 cells. *BMC Complement Altern Med*. 2017;17(1):244.
[PUBMED](#) | [CROSSREF](#)
22. Qin SY. Complete genome analysis and biological characteristics of PRV GXLB-2015 and GXGG-2016 strain [Master's dissertation]. Nanning: Guangxi University; 2017.
23. Pomeranz LE, Reynolds AE, Hengartner CJ. Molecular biology of pseudorabies virus: impact on neurovirology and veterinary medicine. *Microbiol Mol Biol Rev*. 2005;69(3):462-500.
[PUBMED](#) | [CROSSREF](#)
24. Laval K, Vernejoul JB, Van Cleemput J, Koyuncu OO, Enquist LW. Virulent pseudorabies virus infection induces a specific and lethal systemic inflammatory response in mice. *J Virol*. 2018;92(24):e01614-18.
[PUBMED](#) | [CROSSREF](#)
25. Poeck H, Ruland J. From virus to inflammation: mechanisms of RIG-I-induced IL-1 β production. *Eur J Cell Biol*. 2012;91(1):59-64.
[PUBMED](#) | [CROSSREF](#)
26. Tisoncik JR, Korth MJ, Simmons CP, Farrar J, Martin TR, Katze MG. Into the eye of the cytokine storm. *Microbiol Mol Biol Rev*. 2012;76(1):16-32.
[PUBMED](#) | [CROSSREF](#)
27. Turner MD, Nedjai B, Hurst T, Pennington DJ. Cytokines and chemokines: at the crossroads of cell signalling and inflammatory disease. *Biochim Biophys Acta*. 2014;1843(11):2563-2582.
[PUBMED](#) | [CROSSREF](#)
28. Ohashi W, Hattori K, Hattori Y. Control of macrophage dynamics as a potential therapeutic approach for clinical disorders involving chronic inflammation. *J Pharmacol Exp Ther*. 2015;354(3):240-250.
[PUBMED](#) | [CROSSREF](#)
29. Miller LC, Zanella EL, Waters WR, Lager KM. Cytokine protein expression levels in tracheobronchial lymph node homogenates of pigs infected with pseudorabies virus. *Clin Vaccine Immunol*. 2010;17(5):728-734.
[PUBMED](#) | [CROSSREF](#)
30. Rahman I. Oxidative stress, transcription factors and chromatin remodelling in lung inflammation. *Biochem Pharmacol*. 2002;64(5-6):935-942.
[PUBMED](#) | [CROSSREF](#)
31. Hensley K, Robinson KA, Gabbita SP, Salsman S, Floyd RA. Reactive oxygen species, cell signaling, and cell injury. *Free Radic Biol Med*. 2000;28(10):1456-1462.
[PUBMED](#) | [CROSSREF](#)
32. Guzik TJ, Korbut R, Adamek-Guzik T. Nitric oxide and superoxide in inflammation and immune regulation. *J Physiol Pharmacol* 2003;54(4):469-487.
[PUBMED](#)
33. Chen L, Kang YH. Antioxidant and enzyme inhibitory activities of Plebeian herba (*Salvia plebeia* R. Br.) under different cultivation conditions. *J Agric Food Chem*. 2014;62(10):2190-2197.
[PUBMED](#) | [CROSSREF](#)
34. Gopez JJ, Yue H, Vasudevan R, Malik AS, Fogelsanger LN, Lewis S, et al. Cyclooxygenase-2-specific inhibitor improves functional outcomes, provides neuroprotection, and reduces inflammation in a rat model of traumatic brain injury. *Neurosurgery*. 2005;56(3):590-604.
[PUBMED](#) | [CROSSREF](#)
35. Jang SI, Kim BH, Lee WY, An SJ, Choi HG, Jeon BH, et al. Stylopine from *Chelidonium majus* inhibits LPS-induced inflammatory mediators in RAW 264.7 cells. *Arch Pharm Res*. 2004;27(9):923-929.
[PUBMED](#) | [CROSSREF](#)
36. Talar-Wojnarowska R, Gasiorowska A, Smolarz B, Romanowicz-Makowska H, Kulig A, Malecka-Panas E. Clinical significance of interleukin-6 (IL-6) gene polymorphism and IL-6 serum level in pancreatic adenocarcinoma and chronic pancreatitis. *Dig Dis Sci*. 2009;54(3):683-689.
[PUBMED](#) | [CROSSREF](#)
37. Brandt J, Haibel H, Cornely D, Golder W, Gonzalez J, Reddig J, et al. Successful treatment of active ankylosing spondylitis with the anti-tumor necrosis factor alpha monoclonal antibody infliximab. *Arthritis Rheum*. 2000;43(6):1346-1352.
[PUBMED](#) | [CROSSREF](#)
38. McCoy MK, Tansey MG. TNF signaling inhibition in the CNS: implications for normal brain function and neurodegenerative disease. *J Neuroinflammation*. 2008;5(1):45.
[PUBMED](#) | [CROSSREF](#)

39. Wilson MR, Choudhury S, Takata M. Pulmonary inflammation induced by high-stretch ventilation is mediated by tumor necrosis factor signaling in mice. *Am J Physiol Lung Cell Mol Physiol*. 2005;288(4):L599-L607.
[PUBMED](#) | [CROSSREF](#)
40. Ogando DG, Paz D, Cella M, Franchi AM. The fundamental role of increased production of nitric oxide in lipopolysaccharide-induced embryonic resorption in mice. *Reproduction*. 2003;125(1):95-110.
[PUBMED](#) | [CROSSREF](#)
41. O'Neill E, Griffin ÉW, O'Sullivan R, Murray C, Ryan L, Yssel J, et al. Acute neuroinflammation, sickness behavior and working memory in response to acute systemic challenge with LPS following noradrenergic lesion in mice. *Brain Behav Immun* 2020;8:S0889-1591(20)32445-4.
[PUBMED](#)
42. Fuijkschot WW, Morrison MC, Zethof IP, Krijnen PA, Kleemann R, Niessen HW, et al. LPS-induced systemic inflammation does not alter atherosclerotic plaque area or inflammation in APOE3*LEIDEN mice in the early phase up to 15 days. *Shock*. 2018;50(3):360-365.
[PUBMED](#) | [CROSSREF](#)